Eur. Phys. J. B **4**, 1–11 (1998)

THE EUROPEAN PHYSICAL JOURNAL B

Calculation of X-ray natural circular dichroism

C.R. Natoli[1], Ch. Brouder[2,a], Ph. Sainctavit[2], J. Goulon[3], Ch. Goulon-Ginet[3,b], and A. Rogalev[3]

[1] Laboratori Nazionali di Frascati dell'Istituto Nazionale di Fisica Nucleare, PO Box 13, 00044 Frascati, Italy
[2] Laboratoire de Minéralogie Cristallographie, Universités Paris VI, Paris VII, Case 115, 4 place Jussieu, 75252 Paris Cedex 05, France
[3] European Synchrotron Radiation Facility, BP 220, 38043, Grenoble Cedex, France

Received: 20 October 1997 / Revised: 18 February 1998 / Accepted: 31 March 1998

Abstract. A method is presented to calculate the natural circular dichroism recently discovered in the X-ray range (XNCD). The basic formula represents XNCD as an odd second-rank tensor and leads to a sum rule that relates XNCD to the mixing of odd and even orbitals in the ground state. A multiple-scattering theory of XNCD is presented, and calculated spectra for the L-edges of iodine in $LiIO_3$ compare favorably with the experiments.

PACS. 33.55.Ad Optical activity, optical rotation; circular dichroism – 71.15.Cr Scattering methods – 78.70.Dm X-ray absorption spectra

1 Introduction

Very recently, natural circular dichroism was measured in the X-ray range, in an inorganic non-centrosymmetric single crystal ($LiIO_3$) [1] and in a stereogenic organometallic complex [2]. In both references, it was observed that XNCD arises from the interference of electric dipole and electric quadrupole transitions. Therefore, the existence of XNCD is possible only when final states mix even and odd orbitals. This mixing of even and odd orbitals is also the driving mechanism of optical transitions in 3d ions and is responsible for the colour intensity of many glasses and minerals. Since the calculation of optical transition intensities in transition metal ions is still in its infancy it is important to have a measure of this mixing. We think that XNCD can provide such a measure.

The derivation of a practical expression for the XNCD cross-section led us to establish a sum rule for XNCD that relates the intensity of XNCD to the even-odd orbital mixing in the initial state. Then, a multiple-scattering theory of XNCD is established, and detailed expressions are given for the K- and L-edges, with real and complex spherical harmonics. Finally, multiple-scattering calculations are carried out for the L_I and L_{III} edges of iodine in $LiIO_3$, and compared with experiments.

[a] e-mail: `brouder@lmcp.jussieu.fr`
[b] Also: Université Joseph Fourier 1, Faculté de Pharmacie, BP 53, 38041 Grenoble Cedex 9, France.

2 The XNCD cross-section

The basic aspects of natural circular dichroism in the X-ray range were given in reference [3], where it was established that the interference between electric dipole and electric quadrupole transitions was the most important mechanism because magnetic dipole transitions were negligible. The smallness of magnetic dipole transitions was confirmed in references [2,4] (see, however, Ref. [5]). Building on this, we write the absorption cross-section in terms of electric dipole and quadrupole transitions as [6]:

$$\sigma(\hat{\epsilon}) = 4\pi^2\alpha_0\hbar\omega \times \sum_f |\langle f|\,(\hat{\epsilon}\cdot\mathbf{r}) + \frac{i}{2}(\hat{\epsilon}\cdot\mathbf{r})\,(\mathbf{k}\cdot\mathbf{r})\,|g\rangle|^2\delta(E_f - E_i - \hbar\omega),$$

where $\hat{\epsilon}$ is the X-ray polarization vector, $\mathbf{k}$ the X-ray wavevector, $|g\rangle$ and $|f\rangle$ the initial and final states with energies E_f and E_i, $\hbar\omega$ the X-ray energy and α_0 the fine structure constant. For notational convenience, we use one-electron wavefunctions. However, all results of Sections 2 and 3 remain true with many-body initial and final states. The only difference is that $\hat{\epsilon}\cdot\mathbf{r}$ becomes $\sum_i \hat{\epsilon}\cdot\mathbf{r}_i$ and $(\hat{\epsilon}\cdot\mathbf{r})(\mathbf{k}\cdot\mathbf{r})$ becomes $\sum_i(\hat{\epsilon}\cdot\mathbf{r}_i)(\mathbf{k}\cdot\mathbf{r}_i)$. We use one-electron wavefunctions to avoid the presence of additional summations and indices.

Our approach does not take relativistic effects into account. Therefore, if the reader is interested in absolute cross-sections, she or he must multiply all cross-section

formulas by 2 (the spin degeneracy) for a K or an L_I-edge, by 2/3 for an L_{II}-edge, by 4/3 for an L_{III}-edge, and more generally by $(2j+1)/(2\ell_0+1)$ for a core hole with orbital momentum ℓ_0 and total angular momentum $j = \ell_0 \pm 1/2$. This accounts for the spin-orbit interaction on the core state, and we neglect the spin-orbit interaction on the photoelectron state.

For simplicity, we consider a fully (elliptically) polarized incident X-ray beam. The spectra corresponding to partially polarized beams can be obtained from our formulas by considering the partially polarized beam as the sum of two fully polarized beams [7].

2.1 Derivation of the XNCD cross-section

In the present paper, we assume that the sample is non magnetic, so that the initial and final state wavefunctions can be chosen real. For magnetic samples, additional terms would appear in the cross-section.

With this assumption we can write the natural circular dichroism cross-section as:

$$\begin{aligned}\sigma_{NCD} &= \sigma(\hat{\epsilon}) - \sigma(\hat{\epsilon}^*) \\ &= -8\pi^2\alpha_0\hbar\omega \sum_f \Im\left[\langle g|\hat{\epsilon}^*\cdot\mathbf{r}|f\rangle\langle f|\hat{\epsilon}\cdot\mathbf{r}\,\mathbf{k}\cdot\mathbf{r}|g\rangle\right] \\ &\quad\times \delta(E_f - E_i - \hbar\omega).\end{aligned}$$

At this stage, it is convenient to remark that $\hat{\epsilon}^*\cdot\mathbf{r}$ is odd and $\hat{\epsilon}\cdot\mathbf{r}\,\mathbf{k}\cdot\mathbf{r}$ is even under the inversion $\mathbf{r}\to-\mathbf{r}$, so that σ_{NCD} is odd under inversion. Consequently, there is no natural circular dichroism if the sample has a center of symmetry.

For definiteness, we could choose the z-axis along the X-ray beam direction ($\mathbf{k}\cdot\mathbf{r} = kz$) and the polarization convention used for X-ray magnetic circular dichroism, where the spectrum is obtained as the difference between right (helicity $-\hbar$) and left (helicity $+\hbar$) polarizations, so that $\hat{\epsilon}\cdot\mathbf{r} = (x-iy)/\sqrt{2}$. In that case, the XNCD cross-section takes the simple form:

$$\begin{aligned}\sigma_{NCD} = 4\pi^2\alpha_0\hbar\omega k \sum_f &\left[\langle g|x|f\rangle\langle f|yz|g\rangle\right. \\ &\left.-\langle g|y|f\rangle\langle f|xz|g\rangle\right]\delta(E_f - E_i - \hbar\omega).\end{aligned}$$

However, since we want to investigate the angular dependence of XNCD, we have to consider a general polarization vector $\hat{\epsilon}$ and X-ray direction $\mathbf{k}$. It is convenient to write

$$\begin{aligned}\hat{\epsilon}\cdot\mathbf{r} &= \frac{4\pi}{3} r \sum_\lambda (-1)^\lambda Y_1^{-\lambda}(\hat{\epsilon}) Y_1^\lambda(\hat{r}) \\ \hat{\epsilon}^*\cdot\mathbf{r} &= \frac{4\pi}{3} r \sum_{\lambda'} (-1)^{\lambda'} Y_1^{-\lambda'}(\hat{\epsilon}^*) Y_1^{\lambda'}(\hat{r}) \\ \mathbf{k}\cdot\mathbf{r} &= \frac{4\pi}{3} kr \sum_\mu (-1)^\mu Y_1^{-\mu}(\hat{k}) Y_1^\mu(\hat{r}),\end{aligned}$$

where $Y_\ell^m(\hat{u})$ are spherical harmonics (with the Condon and Shortley phase convention) evaluated at the angles determining the unit vector $\hat{u}$ [8].

By recoupling the spherical harmonics $Y_1^\lambda(\hat{r})$ and $Y_1^\mu(\hat{r})$ we obtain (Ref. [9], p. 156)

$$\begin{aligned}\hat{\epsilon}\cdot\mathbf{r}\,\mathbf{k}\cdot\mathbf{r} = &\left(\frac{4\pi}{3}\right)^2 k\sqrt{\frac{3}{10\pi}} \\ &\times \sum_{\lambda\mu\nu} (-1)^\nu Y_1^{-\lambda}(\hat{\epsilon}) Y_1^{-\mu}(\hat{k}) (1\lambda1\mu|2\nu) r^2 Y_2^\nu(\hat{r}),\end{aligned}$$

where $(1\lambda1\mu|2\nu)$ is a Clebsch-Gordan coefficient [9].

Bringing the terms together yields

$$\begin{aligned}\sigma_{NCD} = &-8\pi^2\alpha_0\hbar\omega\left(\frac{4\pi}{3}\right)^3 k\sqrt{\frac{3}{10\pi}} \\ &\times \Im\Big[\sum_{\lambda\mu\nu\lambda'} (-1)^{\nu+\lambda'} Y_1^{-\lambda}(\hat{\epsilon}) Y_1^{-\mu}(\hat{k}) Y_1^{-\lambda'}(\hat{\epsilon}^*) \\ &\times (1\lambda1\mu|2\nu) \sum_f \langle g|r Y_1^{\lambda'}(\hat{r})|f\rangle\langle f|r^2 Y_2^\nu(\hat{r})|g\rangle\Big] \\ &\times \delta(E_f - E_i - \hbar\omega).\end{aligned}$$

At this point, we use the fact that the wavefunctions can be chosen real, so that initial and final states can be interchanged (*e.g.* $\langle f|\hat{\epsilon}\cdot\mathbf{r}|g\rangle = \langle g|\hat{\epsilon}\cdot\mathbf{r}|f\rangle$).

By writing $\Im[\,] = (-i/2)[\,] + (i/2)[\,]^*$ the imaginary part of the previous expression becomes

$$\begin{aligned}-\frac{i}{2}\sum_{\lambda\mu\nu\lambda'} (-1)^{\nu+\lambda'} &\Big[Y_1^{-\lambda}(\hat{\epsilon}) Y_1^{-\lambda'}(\hat{\epsilon}^*) \\ &- Y_1^{-\lambda'}(\hat{\epsilon}) Y_1^{-\lambda}(\hat{\epsilon}^*)\Big] Y_1^{-\mu}(\hat{k}) (1\lambda1\mu|2\nu) \\ &\sum_f \langle g|r Y_1^{\lambda'}(\hat{r})|f\rangle\langle f|r^2 Y_2^\nu(\hat{r})|g\rangle.\end{aligned}$$

Using Section 3.2.1 of reference [10], it can be proved that

$$\begin{aligned}Y_1^{-\lambda}(\hat{\epsilon}) Y_1^{-\lambda'}(\hat{\epsilon}^*) - Y_1^{-\lambda'}(\hat{\epsilon}) Y_1^{-\lambda}(\hat{\epsilon}^*) = \\ -\sqrt{\frac{3}{2\pi}} P_c \sum_{\mu'} (1-\lambda1-\lambda'|1\mu') Y_1^{\mu'}(\hat{k}),\end{aligned}$$

where $(1-\lambda1-\lambda'|1\mu')$ is a Clebsch-Gordan coefficient and P_c is the rate of circular polarization defined by $\hat{\epsilon}\times\hat{\epsilon}^* = iP_c\hat{k}$. Note that P_c is positive for a right circular polarization in the traditional sense [11] (*i.e.* for a negative helicity).

Finally, the spherical harmonic $Y_1^{\mu'}(\hat{k})$ is recoupled to the $Y_1^{-\mu}(\hat{k})$ coming from the electric quadrupole operator, the sum of products of three Clebsch-Gordan coefficients

Table 1. Angular dependence of XNCD and absorption for the allowed point groups.

Point Group	XNCD	Absorption
D_6, C_6, D_4, C_4, D_3, C_3	σ_1	σ_a
D_{2d}	σ_2	σ_a
C_{2v}	σ_3	σ_b
S_4	$\sigma_2+\sigma_3$	σ_a
D_2	$\sigma_1+\sigma_2$	σ_b
C_{1h}	σ_4	σ_c
C_2	$\sigma_1+\sigma_2+\sigma_3$	σ_c
C_1	$\sigma_1+\sigma_2+\sigma_3+\sigma_4$	$\sigma_c+\sigma_d$

is rewritten as the product of a 6-j symbol and a Clebsch-Gordan coefficient (see Ref. [9], p. 108) and we obtain our final form for the natural circular dichroism cross-section:

$$\sigma_{NCD} = -8\pi^2\alpha_0\hbar\omega\left(\frac{4\pi}{3}\right)^{3/2} k\sqrt{\frac{3}{2}}\frac{P_c}{5} \times \sum_{\lambda\mu\nu} Y_2^{\nu *}(\hat{k})(1\lambda 2\mu|2\nu) \times i\sum_f \langle g|rY_1^\lambda(\hat{r})|f\rangle\langle f|r^2Y_2^\mu(\hat{r})|g\rangle\delta(E_f-E_i-\hbar\omega). \quad (1)$$

As will be clear in the next sections, expression (1) is well suited to the derivation of sum rules and multiple-scattering formulas.

2.2 Symmetry and spectral shapes

If we use the notation

$$\sigma^{(\nu)} = -8\pi^2\alpha_0\hbar\omega\left(\frac{4\pi}{3}\right)^{3/2} k\sqrt{\frac{3}{2}}\frac{1}{5}\sum_{\lambda\mu}(1\lambda 2\mu|2\nu) \times i\sum_f \langle g|rY_1^\lambda(\hat{r})|f\rangle\langle f|r^2Y_2^\mu(\hat{r})|g\rangle\delta(E_f-E_i-\hbar\omega),$$

the natural circular dichroism writes

$$\sigma_{NCD} = P_c\sum_\nu Y_2^{\nu *}(\hat{k})\sigma^{(\nu)},$$

where $\sigma^{(\nu)}$ transforms as the components of an odd rank 2 spherical tensor. From its expression, it can be shown that the tensor components have the following symmetry: $[\sigma^{(\nu)}]^* = (-1)^\nu\sigma^{(-\nu)}$. Therefore, σ_{NCD} is real, as it should be.

Point group symmetries cancel some of the five possible $\sigma^{(\nu)}$. We can apply the same technique as for linear dichroism [6] and calculate, for the point symmetry group G of the sample space group, the tensor components compatible with the symmetry as:

$$\langle\sigma^{(\nu)}\rangle = \frac{1}{|G|}\sum_{R\in G}(-1)^R\sigma^{(\nu')}\mathcal{D}^{(2)}_{\nu'\nu}(R),$$

where $\mathcal{D}^{(2)}_{\nu'\nu}(R)$ is the Wigner rotation matrix corresponding to the rotation part of the symmetry operation R and $(-1)^R$ is 1 if R is a pure rotation and -1 if R is the product of a rotation by an inversion. In this formula, the symmetry operations were applied to the crystal, but identical results are obtained by applying the operations to the spherical harmonics $Y_2^{\nu *}(\hat{k})$.

From this treatment, we can deduce the angular dependence of XNCD spectra. For most symmetry groups, the angular dependence can be summarized by one or two spectral shapes $\sigma^{(\nu)}$. Since the linear dichroism of low symmetry crystals is very complex, angular dependence experiments provide a useful test of the validity of measured XNCD spectra.

We give now a list of the angular dependences of natural circular dichroism as a function of angle. We first define a reference frame bound to the crystal axes. The z-axis is aligned along the c-axis of the crystal and the x-axis is along a direction, in the plane perpendicular to c, defined by another symmetry operation (rotation axis, mirror plane). When no such direction exists, any direction perpendicular to c can be chosen. In this frame, the unit vector $\hat{k}$ has components $(\sin\theta\cos\phi, \sin\theta\sin\phi, \cos\theta)$.

For a given crystal, the point group to consider is not the local point group of the absorbing atom but the point group of the space group. In the following, $\sigma^{(\nu)}$ are spectral shapes, and $\sigma^{(\nu r)}$ ($\sigma^{(\nu i)}$) stands for the real (imaginary) part of $\sigma^{(\nu)}$. The angular dependences of natural circular dichroism for the point groups compatible with XNCD are given in Tables 1 and 2. In Table 2, the angular dependence is given as a function of the angles θ and ϕ, and as a function of the wavevector direction $\hat{k}$.

For completeness, we give the corresponding expression for the electric dipole cross-section, valid for complex polarization vectors. Table 1 gives the angular dependence for the point groups, Table 3 gives the corresponding functions. The electric dipole spectral shapes are defined by [6]

$$\sigma^D(\ell,m) = -\pi\alpha_0\hbar\omega\left(\frac{4\pi}{3}\right)^2\sqrt{3}\sum_{\lambda\mu}(1\lambda 1\mu|\ell m) \times \sum_f \langle g|rY_1^\lambda(\hat{r})|f\rangle\langle f|rY_1^\mu(\hat{r})|g\rangle\delta(E_f-E_i-\hbar\omega).$$

3 XNCD sum rule

We now use the method developed by Thole *et al.* [12–14] to derive a sum rule for the XNCD spectra at specific edges.

We start from equation (1), that we write in a second quantized form, and we use the Wigner-Eckart theorem to

Table 2. Types of angular dependences for XNCD.

	Coordinates	Angles
σ_1	$P_c\sqrt{\frac{5}{16\pi}}(3\hat{k}_z^2-1)\sigma^{(0r)}$	$P_c\sqrt{\frac{5}{16\pi}}(3\cos^2\theta-1)\sigma^{(0r)}$
σ_2	$P_c\sqrt{\frac{15}{8\pi}}(\hat{k}_x^2-\hat{k}_y^2)\sigma^{(2r)}$	$P_c\sqrt{\frac{15}{8\pi}}\sin^2\theta\cos 2\phi\sigma^{(2r)}$
σ_3	$P_c\sqrt{\frac{15}{2\pi}}\hat{k}_x\hat{k}_y\sigma^{(2i)}$	$P_c\sqrt{\frac{15}{8\pi}}\sin^2\theta\sin 2\phi\sigma^{(2i)}$
σ_4	$-P_c\sqrt{\frac{15}{2\pi}}\hat{k}_z(\hat{k}_x\sigma^{(1r)}+\hat{k}_y\sigma^{(1i)})$	$-P_c\sqrt{\frac{15}{8\pi}}\sin 2\theta(\cos\phi\sigma^{(1r)}+\sin\phi\sigma^{(1i)})$

Table 3. Types of angular dependences for absorption.

	Coordinates
σ_a	$\sigma^D(0,0)-1/\sqrt{2}(3\lvert\epsilon_z\rvert^2-1)\sigma^D(2,0)$
σ_b	$\sigma_a-\sqrt{3}(\lvert\epsilon_x\rvert^2-\lvert\epsilon_y\rvert^2)\sigma^{Dr}(2,2)$
σ_c	$\sigma_b-2\sqrt{3}\Re(\epsilon_x\epsilon_y^*)\sigma^{Di}(2,2)$
σ_d	$2\sqrt{3}\Re(\epsilon_x\epsilon_z^*)\sigma^{Dr}(2,1)+2\sqrt{3}\Re(\epsilon_y\epsilon_z^*)\sigma^{Di}(2,1)$

derive

$$\langle g|rY_1^\lambda|f\rangle = \sum_{\ell m\ell_0 m_0}(-1)^{m_0}\sqrt{\frac{(2\ell_0+1)3(2\ell+1)}{4\pi}}\begin{pmatrix}\ell_0 & 1 & \ell\\ 0 & 0 & 0\end{pmatrix}D_\ell \times\begin{pmatrix}\ell_0 & 1 & \ell\\ -m_0 & \lambda & m\end{pmatrix}\langle g|a^+_{\ell_0 m_0}a_{\ell m}|f\rangle$$

$$\langle f|r^2Y_2^\mu|g\rangle = \sum_{\ell' m'\ell_0 m_0'}(-1)^{m'}\sqrt{\frac{(2\ell_0+1)5(2\ell'+1)}{4\pi}}\begin{pmatrix}\ell' & 2 & \ell_0\\ 0 & 0 & 0\end{pmatrix}Q_{\ell'} \times\begin{pmatrix}\ell' & 2 & \ell_0\\ -m' & \mu & m_0'\end{pmatrix}\langle f|a^+_{\ell' m'}a_{\ell_0 m_0'}|g\rangle,$$

where ℓ_0 is the angular momentum of the core hole, and the radial dipole and quadrupole integrals are defined by

$$D_\ell=\int_0^{\rho_{MT}}r^3dr\phi_0(r)R^0_\ell(r)$$
$$Q_{\ell'}=\int_0^{\rho_{MT}}r^4dr\phi_0(r)R^0_{\ell'}(r),$$

where the core state and photoelectron radial muffin-tin wavefunctions are $\phi_0(r)$ and $R^0_\ell(r)$, respectively, and $\phi_0(r)$ is assumed to be localized in the muffin-tin sphere of radius ρ_{MT}. Here, ℓ is the final angular momentum of the dipole transition ($\ell=1$ if $\ell_0=0$, $\ell=0$ or 2 if $\ell_0=1$), and ℓ' that of the quadrupole transition ($\ell'=2$ if $\ell_0=0$, $\ell'=1$ or 3 if $\ell_0=1$). Therefore, ℓ and ℓ' have opposite parity. To avoid any ambiguity, we stress here that the term final angular momentum is an abuse of language. Since the cluster is not spherically symmetric, angular momentum is not a good quantum number and final states are a mixture of many angular momenta. The dipole and quadrupole transition operators pick up, in the final states, the components corresponding to angular momenta ℓ and ℓ'.

Since the normalization procedure of experimental spectra enables us to obtain the absorption spectrum corresponding to a specific core hole angular momentum ℓ_0, we can suppress the sum over ℓ_0.

With this notation, we can use angular momentum algebra to reexpress the sum of products of three 3-j symbols as a product of a 6-j and a 3-j symbols, and the XNCD cross-section becomes:

$$\sigma_{NCD}=8\pi^2\alpha_0\hbar\omega k\sqrt{\frac{2\pi}{15}}P_c(2\ell_0+1) \times\sum_{\ell\ell'}\sqrt{(2\ell+1)(2\ell'+1)}\begin{Bmatrix}2 & \ell' & \ell\\ \ell_0 & 1 & 2\end{Bmatrix}D_\ell Q_{\ell'} \times\begin{pmatrix}\ell & 1 & \ell_0\\ 0 & 0 & 0\end{pmatrix}\begin{pmatrix}\ell' & 2 & \ell_0\\ 0 & 0 & 0\end{pmatrix}\sum_\nu Y_2^{\nu*}(\hat{k})\sigma^\nu_{\ell\ell'} \quad (2)$$

where

$$\sigma^\nu_{\ell\ell'}=i\sum_{mm'\kappa}(-1)^{\ell-m}(\ell-m\ell'm'|2\nu) \times\sum_f\langle g|a^+_{\ell_0\kappa}a_{\ell m}|f\rangle\langle f|a^+_{\ell' m'}a_{\ell_0\kappa}|g\rangle\delta(E_f-E_i-\hbar\omega).$$

The next step towards the derivation of a sum rule is to eliminate the external energy dependent factors so that the integral over energy yields a resolution of identity. Energy appears in equation (2) through $\hbar\omega$ and $k=(\hbar\omega)/(\hbar c)$. Therefore, the sum rule is obtained from the experimental spectrum σ_{NCD} as

$$\Sigma_{NCD}=\int\frac{\sigma_{NCD}}{(\hbar\omega)^2}d(\hbar\omega).$$

Carrying out this integral over energies in equation (2) eliminates the delta function, leaving $\sum_f|f\rangle\langle f|=1$ [15]. The anticommutation relations for the creation-annihilation operators and the fact that the core shell is

full in the initial state lead to the final expression

$$\Sigma_{NCD} = \frac{8\pi^2\alpha_0}{\hbar c}\sqrt{\frac{2\pi}{15}}P_c(2\ell_0+1) \times \sum_{\ell\ell'}\sqrt{(2\ell+1)(2\ell'+1)}\begin{Bmatrix} 2 & \ell' & \ell \\ \ell_0 & 1 & 2\end{Bmatrix} D_\ell Q_{\ell'} \times \begin{pmatrix}\ell & 1 & \ell_0\\ 0&0&0\end{pmatrix}\begin{pmatrix}\ell' & 2 & \ell_0\\ 0&0&0\end{pmatrix}\sum_\nu Y_2^{\nu *}(\hat{k})\langle g|M^\nu_{\ell\ell'}|g\rangle \quad (3)$$

where the operator

$$M^\nu_{\ell\ell'} = i\sum_{mm'}(-1)^{\ell-m}(\ell - m\ell' m'|2\nu)a_{\ell m}a^+_{\ell' m'}$$

measures a mixing of ℓ and ℓ' orbitals in the ground state. Notice that we are speaking here of the many-body ground state $|g\rangle$ and not of the initial core state of the one-body approach. From the Wigner-Eckart theorem, the mixing operator $M^\nu_{\ell\ell'}$ would be proportional to $Y^\nu_2(\hat{r})$ (a quadrupole moment) if ℓ and ℓ' had the same parities. However, the analogy between $M^\nu_{\ell\ell'}$ and a quadrupole moment is misleading, since $M^\nu_{\ell\ell'}$ couples only angular momenta of different parities.

To get some insight into the physical meaning of the operator $M^\nu_{\ell\ell'}$, we first notice that, since $\ell \neq \ell'$, it measures the mixing of different atomic orbitals. Moreover, since the parity corresponding to ℓ and ℓ' is different, the operator measures the orbital mixing caused by the absence of an inversion center in the system.

If we take the example of a molecular orbital

$$|g\rangle = \sum_m c_{\ell m}|\ell m\rangle + \sum_{m'} c_{\ell' m'}|\ell' m'\rangle,$$

then

$$\langle g|M^0_{\ell\ell'}|g\rangle \propto \sum_{m>0} m\sqrt{n^2-m^2}\Im[c_{\ell m}c^*_{\ell' m'}],$$

where $n = \max(\ell, \ell')$.

The meaning of the sum rule (3) is clearer at the K-edge, where $\ell_0 = 0, \ell = 1, \ell' = 2$ and the sum rule becomes

$$\Sigma_{NCD} = \frac{4\pi^2\alpha_0}{\hbar c}\sqrt{\frac{2\pi}{45}}P_c\sum_\nu Y_2^{\nu *}\langle g|M^\nu_{12}|g\rangle D_1 Q_2.$$

Therefore, XNCD measures the mixing of p and d orbitals in the ground state. This parameter is very important for the calculation of the intensity of optical transitions. The measurement of XNCD spectra at the K-edge of transition metal impurities offers a unique independent determination of this parameter.

In the case an L_{II}- or L_{III}-edge the selection rules coming from the the 6-j symbol eliminate the contribution of the dipole transitions towards s states and we are left with $\ell_0 = 1, \ell = 2, \ell' = 3$, and $\ell_0 = 1, \ell = 2, \ell' = 1$ for which the sum rules are

$$\Sigma_{NCD} = \frac{4\pi^2\alpha_0}{\hbar c}\sqrt{\frac{2\pi}{125}}P_c\sum_\nu Y_2^{\nu *}\Big[2\langle g|M^\nu_{23}|g\rangle D_2 Q_3 - \langle g|M^\nu_{21}|g\rangle D_2 Q_1\Big].$$

The application of this sum rule to experimental spectra meets the same difficulties as the sum rule of X-ray magnetic circular dichroism [16]. In particular, the integration bounds have to be chosen carefuly.

4 Multiple-scattering approach

In this section, we specialize to a one-particle approach to XNCD. The Green function approach is used with complex and real spherical harmonics. Both presentations are useful because each brings its own light to the result and because we find useful to discuss an apparent discrepancy between the formulas obtained with complex and real spherical harmonics. Finally, we present the decomposition of XNCD into scattering paths, showing that single scattering does not contribute to it. In this section, we use atomic units ($\hbar = 2m = 1$).

4.1 The Green function approach

In this section, we use the Green function form of the multiple-scattering approach. In equation (1), we make the substitution

$$\sum_f |f\rangle\delta(E_f - E_i - \hbar\omega)\langle f| = -\frac{1}{\pi}\Im[G(E_i+\hbar\omega)] = \frac{i}{2\pi}[G(E_i+\hbar\omega) - G^*(E_i+\hbar\omega)].$$

Then, we use the expression for the multiple-scattering Green function

$$G(\mathbf{r}_i, \mathbf{r}'_j; z) = -i\sum_{\ell m} t^i_\ell R^i_\ell(r_<)Y^m_\ell(\hat{r}_i)H^i_\ell(r_>)Y^{m*}_\ell(\hat{r}'_i)\delta_{i,j} + \sum_{\ell m\ell' m'} R^i_\ell(r_i)Y^m_\ell(\hat{r}_i)(\tau^{ij}_{\ell m\ell' m'} + t^i_\ell\delta_{\ell,\ell'}\delta_{m,m'}\delta_{i,j}) \times R^j_{\ell'}(r'_j)Y^{m'*}_{\ell'}(\hat{r}'_j) \quad (4)$$

where $\kappa = \sqrt{z}$, δ^i_ℓ is the (complex) phase-shift for potential $V^i(r)$, $t^i_\ell = \sin\delta^i_\ell \exp i\delta^i_\ell$, $R^i_\ell(r)$ is the regular solution of the radial Schrödinger equation for potential $V^i(r)$ that matches smoothly to $\sqrt{\kappa}(\cot\delta^i_\ell j_\ell(\kappa r) - n_\ell(\kappa r))$ at the muffin-tin radius ρ_i, $H^i_\ell(r)$ is the irregular solution of the radial Schrödinger equation for potential $V^i(r)$ that matches smoothly to $\sqrt{\kappa}h^+_\ell(\kappa r)$ at the muffin-tin radius. Finally $\tau^{ij}_{\ell m\ell' m'}$ are the matrix elements of the multiple-scattering matrix $\tau = [T_a^{-1} - H]^{-1}$, where $(T_a)^{ij}_{\ell m\ell' m'} = -t^i_\ell\delta_{i,j}\delta_{\ell,\ell'}\delta_{m,m'}$ and $H^{ij}_{\ell m\ell' m'} = -4\pi i\sum_{\lambda\mu} i^{\ell+\lambda-\ell'}C^{\ell' m'}_{\ell m\lambda\mu}h^+_\lambda(\kappa R_{ij})Y^\mu_\lambda(\hat{R}_{ij})$. In the last expression, the Hankel function h^+_λ is defined as the function $h^{(1)}_\lambda$ of reference [17]. The site $i = 0$ is the absorbing site.

Equation (4) for the Green function enables us to use the Wigner-Eckart theorem in equation (1). This leads to:

$$\sigma_{NCD} = -4\pi\alpha_0^2\omega^2\sqrt{\frac{2\pi}{15}}P_c(2\ell_0+1) \times \sum_{\ell\ell'}\begin{pmatrix}\ell & 1 & \ell_0\\ 0 & 0 & 0\end{pmatrix}\begin{pmatrix}\ell' & 2 & \ell_0\\ 0 & 0 & 0\end{pmatrix}\begin{Bmatrix}2 & \ell' & \ell\\ \ell_0 & 1 & 2\end{Bmatrix} \times \sqrt{(2\ell+1)(2\ell'+1)}D_\ell Q_{\ell'}\Re\Big[\sum_\nu Y_2^{\nu *}(\hat{k})\tau^{00}(\ell\ell';2\nu)\Big]. \quad (5)$$

We recall that [18]

$$\tau^{00}(\ell\ell',a\alpha) = \sum_{mm'}(-1)^{(\ell-m)}(\ell - m\ell' m'|a\alpha)\tau^{00}_{\ell m\ell' m'}.$$

The presence of a real part in the XNCD cross-section is surprising, since we have started from the imaginary part of the Green function. It will be explained in Section 4.3.

4.2 K-, L- and M-edges in complex spherical harmonics

It can be useful to evaluate the absorption and NCD cross-sections for specific edges. To express the absorption cross-section for an elliptically polarized beam, we use the coupled tensor $[\hat{\epsilon}\otimes\hat{\epsilon}^*]^{(2)}_\nu$ defined by Varshalovich *et al.* (Ref. [10], p. 66). When the wavevector is along Oz, the only non-zero coupled tensor is $[\hat{\epsilon}\otimes\hat{\epsilon}^*]^{(2)}_0 = (3|\epsilon_z|^2-1)/\sqrt{6}$ [19].

For a K- or an L_I-edge the absorption cross-section is

$$\sigma_D = -\frac{4\pi\alpha_0\omega}{3\sqrt{3}}D_1^2\Im\Big[\tau^{00}(11;00) - \sqrt{3}\sum_\nu(-1)^\nu[\hat{\epsilon}\otimes\hat{\epsilon}^*]^{(2)}_{-\nu}\tau^{00}(11;2\nu)\Big]$$

and the XNCD cross-section is

$$\sigma_{NCD} = -\frac{4\pi\alpha_0^2\omega^2}{15}\sqrt{2\pi}P_cD_1Q_2 \times\Re\Big[\sum_\nu Y_2^{\nu *}(\hat{k})\tau^{00}(12;2\nu)\Big]. \quad (6)$$

For an L_{II}- or L_{III}-edge, we must take into account dipole transitions towards d and s states. The electric dipole absorption cross-section for d final states is:

$$\sigma_D = -\frac{8\pi\alpha_0\omega}{3\sqrt{5}}D_2^2\Im\Big[\tau^{00}(22;00) - \sqrt{\frac{21}{20}}\sum_\nu(-1)^\nu[\hat{\epsilon}\otimes\hat{\epsilon}^*]^{(2)}_{-\nu}\tau^{00}(22;2\nu)\Big].$$

For s final states,

$$\sigma_D = -\frac{4\pi\alpha_0\omega}{3}D_0^2\Im\Big[\tau^{00}(00;00)\Big].$$

For the interference between s and d final states

$$\sigma_D = -\frac{16\pi\alpha_0\omega}{\sqrt{30}}D_0D_2 \times\Im\Big[\sum_\nu(-1)^\nu[\hat{\epsilon}\otimes\hat{\epsilon}^*]^{(2)}_{-\nu}\tau^{00}(20;2\nu)\Big].$$

For XNCD, the selection rules due to the 6-j symbol in equation (5) show that the dipole transitions to s-states do not intervene and the XNCD cross-section is

$$\sigma_{NCD} = -\frac{4\pi\alpha_0^2\omega^2}{25}\sqrt{2\pi}P_cD_2 \times\Re\Big[\sum_\nu Y_2^{\nu *}(\hat{k})\Big(2Q_3\tau^{00}(23;2\nu) - Q_1\tau^{00}(21;2\nu)\Big)\Big]. \quad (7)$$

In equation (7), the term $2Q_3\tau^{00}(23;2\nu)$ corresponds to $\ell'=3$ and measures the f states reached by quadrupole transitions, the term $-Q_1\tau^{00}(21;2\nu)$ corresponds to $\ell'=1$ and measures the p states reached by quadrupole transitions.

Because of the symmetry relation $\tau^{00}(21;2\nu) = \tau^{00}(12;2\nu)$ [20], we see that the XNCD cross-section at the L_I-edge (Eq. (6)) is proportional to the component of the XNCD cross-section at the $L_{II,III}$-edges which corresponds to quadrupole transitions towards p-states (the second term of Eq. (7)). When the absorption spectra are normalized to one far from the edge, the p-component of XNCD at the $L_{II,III}$-edge of iodine in $LiIO_3$ was found to be of the same shape, but around 14 times smaller than the XNCD spectrum at the L_I-edge, and of opposite sign (see Sect. 5).

For an M_{IV}- or M_V-edge, we must take into account dipole transitions towards f and p states. The electric dipole absorption cross-section for f final states is:

$$\sigma_D = -\frac{4\pi\alpha_0\omega}{\sqrt{7}}D_3^2\Im\Big[D_3^2\tau^{00}(33;00) - \frac{3\sqrt{2}}{5}\sum_\nu(-1)^\nu[\hat{\epsilon}\otimes\hat{\epsilon}^*]^{(2)}_{-\nu}\tau^{00}(33;2\nu)\Big].$$

For p final states,

$$\sigma_D = -\frac{8\pi\alpha_0\omega}{3\sqrt{3}}D_1^2\Im\Big[\tau^{00}(11;00) - \frac{\sqrt{3}}{10}\sum_\nu(-1)^\nu[\hat{\epsilon}\otimes\hat{\epsilon}^*]^{(2)}_{-\nu}\tau^{00}(11;2\nu)\Big].$$

For the interference between p and f final states

$$\sigma_D = -\frac{8\pi\alpha_0\omega\sqrt{6}}{5}D_1D_3 \times\Im\Big[\sum_\nu(-1)^\nu[\hat{\epsilon}\otimes\hat{\epsilon}^*]^{(2)}_{-\nu}\tau^{00}(13;2\nu)\Big].$$

For the natural circular dichroism cross-section, two contributions are relevant. The first one corresponds to dipole

transitions towards p-states:

$$\sigma^1_{NCD} = \frac{4\pi\alpha_0^2\omega^2}{15}\sqrt{2\pi}P_c D_1 Q_2 \times \Re\Big[\sum_\nu Y_2^{\nu *}(\hat{k})\tau^{00}(12;2\nu)\Big],$$

and looks very much like the dichroism at the K-edge (apart from the sign). The second one corresponds to dipole transitions towards f-states:

$$\sigma^2_{NCD} = \frac{8\pi\alpha_0^2\omega^2}{35}\sqrt{2\pi}P_c D_3 \Re\Big[\sum_\nu Y_2^{\nu *}(\hat{k}) \times\Big(Q_2\tau^{00}(32;2\nu) - \sqrt{\frac{5}{2}}Q_4\tau^{00}(34;2\nu)\Big)\Big]. \quad (8)$$

Here the first term looks like the first contribution to the $L_{II,III}$-edge spectra, the second term gives information on the mixing of f and g states in the continuum.

4.3 K- and L-edges in real spherical harmonics

In practice, multiple-scattering programs use real spherical harmonics, defined, for $m > 0$, as cosine spherical harmonics $Y_\ell^{mc} = (Y_\ell^m + Y_\ell^{m*})/\sqrt{2}$ and sine spherical harmonics $Y_\ell^{ms} = (Y_\ell^m - Y_\ell^{m*})/(\sqrt{2}i)$. For definiteness, we consider a right-circularly polarized X-ray beam along Oz ($\hat{\epsilon}\cdot\mathbf{r} = (x-iy)/\sqrt{2}$).

For a K- or an L_I-edge the absorption cross-section is

$$\sigma_D = -\frac{2\pi\alpha_0\omega}{3}D_1^2\Im\Big[\tau^{00}_{11c\,11c} + \tau^{00}_{11s\,11s}\Big]$$

and the XNCD cross-section is

$$\sigma_{NCD} = -\frac{2\pi\alpha_0^2\omega^2}{3\sqrt{5}}D_1Q_2\Im\Big[\tau^{00}_{11c\,21s} - \tau^{00}_{11s\,21c}\Big].$$

For an L_{II}- or L_{III}-edge, the absorption cross-section is (for the dipole transitions to d states)

$$\sigma_D = -\frac{2\pi\alpha_0\omega}{15}D_2^2\Im\Big[2\tau^{00}_{20\,20} + 3\tau^{00}_{21c\,21c} + 3\tau^{00}_{21s\,21s} + 6\tau^{00}_{22c\,22c} + 6\tau^{00}_{22s\,22s}\Big]$$

and the XNCD cross-section is

$$\sigma_{NCD} = -\frac{4\pi\alpha_0^2\omega^2}{5\sqrt{5}}D_2\Im\Big[Q_1\Big(\tau^{00}_{21c\,11s} - \tau^{00}_{21s\,11c}\Big) + 2\sqrt{\frac{5}{7}}Q_3\Big(\tau^{00}_{22c\,32s} - \tau^{00}_{22s\,32c} + \sqrt{\frac{2}{5}}\tau^{00}_{21c\,31s} - \sqrt{\frac{2}{5}}\tau^{00}_{21s\,31c}\Big)\Big].$$

With real spherical harmonics, the absorption cross-section is given in terms of the imaginary part of the multiple-scattering matrix, whereas the real part is used in the complex spherical harmonics. The reason for this is simply that the basis change introduces a factor i. More precisely:

$$\tau^{00}_{\ell mc\,\ell' ms} - \tau^{00}_{\ell ms\,\ell' mc} = -i(\tau^{00}_{\ell m\,\ell' m} - \tau^{00}_{\ell -m\,\ell' -m}).$$

4.4 Wavefunction approach

It is possible to connect the Green function approach to the wavefunction approach through the generalized optical theorem [21]. It is convenient to start from the second quantized expression (2) and to write the final states (in real spherical harmonics and in the one-electron approximation) as

$$|f\rangle = \sum_{\ell m\alpha} B^0_{\ell m\alpha}(\hat{\kappa};\omega)a^+_{\ell m\alpha}a_{\ell_0 m_0\alpha_0}|g\rangle,$$

where $B^0_{\ell m\alpha}(\hat{\kappa};\omega)$ is the multiple-scattering component, over the $\ell m\alpha$ basis ($\alpha = c, s$), of the photoelectron wavefunction corresponding to an outgoing electronic plane wave along $\hat{\kappa}$.

Then, the matrix elements in equation (2) becomes

$$\int d\hat{\kappa}B^0_{\ell m\alpha}(\hat{\kappa};\omega)B^{0*}_{\ell' m'\alpha'}(\hat{\kappa};\omega) = \Im\tau^{00}_{\ell m\alpha\ell' m'\alpha'},$$

because of the optical theorem. For $\ell' = \ell$, the right-hand side would be proportional to the ℓ density of states on the absorbing site. Therefore, for the case of XNCD, we obtain a kind of ℓ, ℓ' cross-density of states on the absorber.

4.5 Expansion into scattering paths

In this section, the full multiple-scattering tensor $\tau^{00}(\ell\ell';2\nu)$ will be expanded as a multiple-scattering series. From this expansion, it will be shown that single scatterings do not contribute.

In reference [18], the multiple-scattering tensor $\tau^{00}(\ell\ell';2\nu)$ was written as a multiple-scattering series

$$\tau^{00}(\ell\ell';2\nu) = \tau^{(2)}(\ell\ell';2\nu) + \tau^{(3)}(\ell\ell';2\nu) + \cdots,$$

where $\tau^{(n)}(\ell\ell';2\nu)$ represents the contribution due to the scattering of the photoelectron by $n-1$ sites of the cluster. In this expansion, the atomic contribution, $\tau^{(0)}(\ell\ell';2\nu)$, is zero because $\ell \neq \ell'$, and the first-order contribution $\tau^{(1)}(\ell\ell';2\nu)$ is zero because the initial and final sites are identical (the absorbing site). It was shown in reference [18] that each term in the series transforms as the full cross-section. In other words, each term of the series shares the same symmetry properties as the full cross-section. Therefore, a scattering path through a set of atoms can contribute to natural circular dichroism only if the symmetries of that set of atoms are compatible with natural circular dichroism.

This remark enables us to eliminate single scattering $\tau^{(2)}(\ell\ell';2\nu)$ from the series. A pair of atoms cannot exhibit natural circular dichroism, because it is possible to find a mirror plane containing the X-ray wavevector and the two atoms. Since this operation changes the helicity of the incoming photon and leaves the two-atom system invariant, the single-scattering process does not contribute to the dichroic signal. This argument using symmetry can

be supplemented by a direct proof. In the notation of reference [18]

$$\tau^{(2)}(\ell\ell';2\nu) = -\, t^0_\ell t^0_{\ell'} \sum_{ab\ell''} O^a_{\ell\ell''}(\kappa R_{0j}) O^b_{\ell''\ell'}(\kappa R_{0j}) t^j_{\ell''} \times (-1)^a \sqrt{(2a+1)(2b+1)} \times W(lal'b; l''2)\langle 2||a||b\rangle Y^\gamma_2(\hat{R}_{0j}).$$

From the definition of $O^a_{\ell\ell''}$ and $O^b_{\ell''\ell'}$ we see that $\ell+a+\ell''$ is even and $\ell'+b+\ell''$ is even. Since $\ell+\ell'$ is odd, this means that $a+b$ is odd. However, $\langle 2||a||b\rangle$ is zero when $a+b$ is odd, so that $\tau^{(2)}(\ell\ell';2\nu)=0$ and the single scattering contribution is zero. Because of this, XNCD is a unique probe of multiple-scattering processes, especially of the influence of disorder on the multiple-scattering contributions.

The first non-zero contribution is the double scattering

$$\tau^{(3)}(\ell\ell';2\nu) = -t^0_\ell t^0_{\ell'} \Xi^3(\ell\ell';2\nu),$$

where $\Xi(\ell\ell';2\nu)$ is defined at the end of page 1498 of reference [18].

The last point we want to stress is that, if the point group of the crystal is not too small, many scattering paths do not contribute to XNCD. The full conditions can be deduced from the list of angular dependences given in Section 2.2 but we give here a useful list of criteria. If a scattering path is transformed into itself (or if paths of the subset transform into one another) by a symmetry operation T then:

- if T is an inversion, the path (subset) does not contribute;
- if T is a rotation by $2\pi/n$ with $n>2$, the path (subset) contributes only to the tensor component $\nu=0$ (Oz is along the rotation axis);
- if T is a rotation by π the path (subset) does not contribute to the tensor components $\nu=\pm1$;
- if T is a mirror whose plane contains or is perpendicular to Oz, then the path (subset) does not contribute to the tensor components $\nu=0$.

The convergence of the multiple-scattering series was tested for $LiIO_3$ and is given in the next section.

5 Calculation of XNCD spectra of $LiIO_3$

The calculation of the XNCD spectra at the L-edges of iodine in $LiIO_3$ where conducted starting from the crystal structure established by Svensson *et al.* [22]. More precisely, we took the space group $P6_3$ (173) with lattice parameters $a=5.481$ Å and $b=5.172$ Å. The atomic positions were taken as Li 2(a) (0,0,0.0764), I 2(b) (1/3,2/3,0) and O 6(c) (0.2471,0.3420,−0.1621). Since the chirality of the sample used in our experiments was unknown, a comparison of calculation and experiment should give us the absolute conformation of our sample.

Calculations were performed in the framework of the MS theory illustrated above, within the muffin-tin approximation and using real spherical harmonics as angular momentum basis functions.

Due to the finite mean free path of the photoelectron in the excited state, the crystal was simulated by a cluster of 40 atoms having a radius of 9 Å around the photoabsorbing iodine atom, slightly more than the average electron mean free path in the energy range considered and enough to reach cluster size convergence.

The Mattheiss prescription [23] was used to construct the cluster electronic density by superposition of neutral atomic charge densities obtained from the Clementi-Roetti tables [24] while the Coulomb part of the potential was obtained by superimposing the corresponding atomic potentials.

In order to simulate the charge relaxation around the core hole in the photoabsorber of atomic number Z, we used the so called screened-relaxed $Z+1$ approximation (final state rule) [25], which consists in taking the orbitals of the $Z+1$ atom with the core electron promoted to the first empty valence orbital for constructing the charge density and potential of the photoabsorber.

For the exchange-correlation part of the potential, we took the energy- and position-dependent complex Hedin-Lundquist (H-L) self energy $\Sigma(\mathbf{r},E)$ [26] as illustrated by Tyson *et al.* (see [27] and references therein). A constant $\Gamma_h/2$, equal to the core hole half width at half maximum, was added to the imaginary part of the H-L potential to take into account the finite core hole lifetime. Altogether the complex part of the potential gives the amplitude attenuation of the excited photoelectronic wave due to extrinsic inelastic losses and the core hole width, and takes automatically into account the photoelectron mean free path in the excited final state. The core hole width was taken equal to 3.5 eV for the L_I edge and 2.7 eV for the L_{III} edge [28].

Finally the muffin-tin radii were chosen according to the criterion of Norman [29], allowing a 15% overlap between contiguous spheres to simulate the atomic bond (the radii were 2.23, 1.69 and 2.30 atomic units for I, O and Li, respectively).

For comparison with experiment, the absorption spectra were normalized to one far from the edge. In the experiments, the X-ray was directed along the c-axis. The intensity of the XNCD spectrum is fixed by the normalization of the absorption spectrum.

The details concerning the experimental set up and the sample used are given in reference [1].

5.1 L_I-edge of iodine

Figure 1 compares the calculated and experimental absorption spectra and XNCD at the L_I-edge of iodine in $LiIO_3$. The agreement is not very good for the absorption spectrum. One notices a contraction of the calculated spectrum as compared to the experimental one. This is an effect of the non-selfconsistency of the charge density. The agreement is better for the XNCD signal. The intensity of the experimental spectra should be multiplied by 1/0.7, so the calculation underestimates the XNCD spectrum. The better agreement for XNCD as compared to absorption is

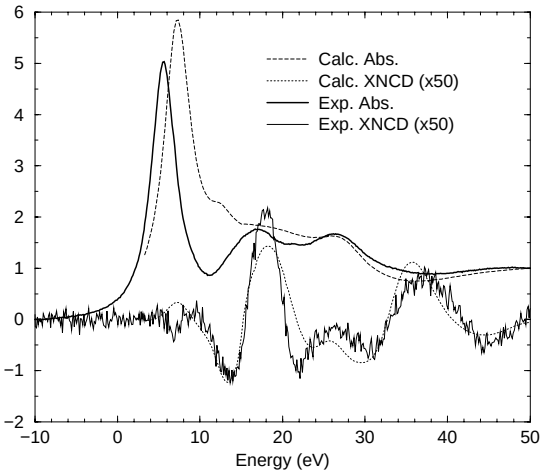

Fig. 1. Experimental (solid line) and calculated (dotted line) absorption and XNCD spectra at the L_I-edge of iodine in $LiIO_3$. The XNCD spectra were multiplied by 50. The calculation was carried out from a sum of neutral atomic charges, with Hedin-Lundqvist exchange and correlation potential.

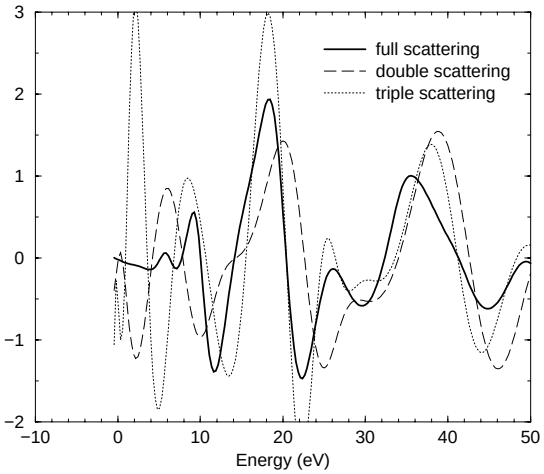

Fig. 2. Comparison of the full multiple-scattering signal (solid line) with the double-scattering contribution (dashed line) and the sum of the double- and triple-scattering contributions (dotted line).

probably due to the molecular and multiple-scattering nature of the XNCD signal. Multiple scattering works well in predicting variations (*e.g.* phase transitions with pressure [30] or temperature [31]) and then gives good agreement for XNCD which is a difference spectrum.

In Figure 1, the calculated XNCD signal was not multiplied by -1, which suggests that the sample has the same chirality as that used in the structural investigation of reference [22].

Finally, the convergence of the expansion of the XNCD cross-section into multiple-scattering contributions is presented in Figure 2. At very low energy, the multiple-scattering series diverges, as is usual, but at higher energy the first multiple-scattering contributions capture the essential features of the XNCD spectrum. Further work is in progress to identify the path contributing most to natural circular dichroism.

5.2 L_{III}-edge of iodine

Figure 3 compares calculated and experimental absorption and XNCD spectra at the L_{III}-edge of iodine in $LiIO_3$. The potential is constructed in a similar way as for the L_I spectrum, except for the $2p$ hole, and core-hole width of 2.7 eV [28]. In the absorption spectrum, the position of the structures is correct, but their intensities does not reproduce well the experimental spectrum. A feature around 10 eV could not be obtained by our calculation. As for the L_I-edge, the agreement is better for XNCD than for absorption and the general shape of the calculated XNCD spectrum reproduces that of the experimental spectrum, except for a background and a peak around 1 eV.

It was established in Section 4 that the XNCD signal is the sum of a contribution due to f states and a contribution due to p states. Figure 4 compares these two contributions. It is clear that the transitions toward p states is very similar to the L_I spectrum (with opposite sign). It should be noticed that the absence of calculated XNCD signal around 1 eV is due to a destructive interference between p and f contributions. Far from the edge, the p contribution becomes small as compared to the f contribution.

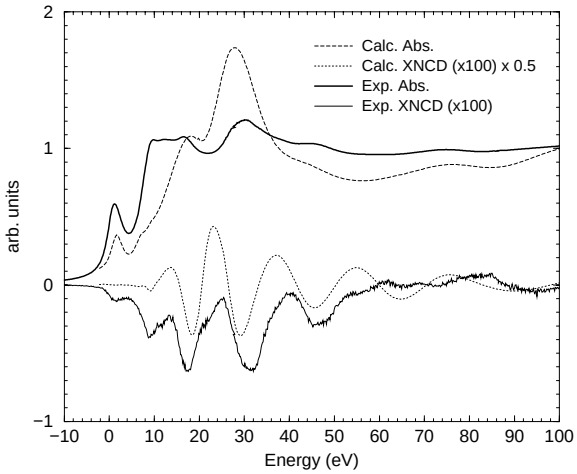

Fig. 3. Experimental (solid line) and calculated (dotted line) absorption and XNCD spectra at the L_{III}-edge of iodine in $LiIO_3$. The experimental XNCD spectrum was multiplied by 100 and the calculated XNCD spectrum by 50. The calculation was carried out from a sum of neutral atomic charges, with Hedin-Lundqvist exchange and correlation potential.

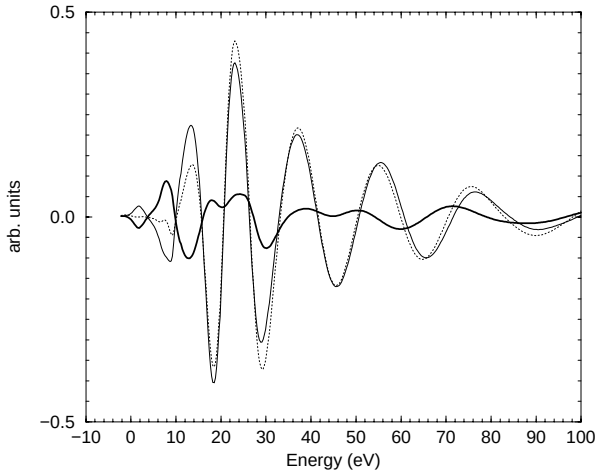

Fig. 4. For the calculated spectrum of Figure 3, full XNCD signal (dotted line), contribution of the quadrupole transitions towards p states (thick solid line) and towards f states (thin solid line).

The large discrepancy between the experimental and calculated absorption spectra might be due to the presence of multielectronic excitations [32].

6 Conclusion

Natural circular dichroism was investigated in the X-ray range. A sum rule was derived and a multiple scattering description of this effect was given. Our first results show that the basic physics of XNCD is understood and the agreement with experiment is sufficient to draw a few preliminary conclusions.

XNCD can be understood within the multiple-scattering formalism. This effect is fully molecular in nature in the sense that it is zero for an isolated atom. Moreover, single scattering does not contribute to it. These two characters of XNCD make it a sensitive probe of the coordination shells surrounding the absorber. The multiple-scattering terms give information on the bond angles and are not mixed with EXAFS signals. These aspects can help measuring the structural relaxation around impurities in single crystals.

XNCD is also determined by a mixing of odd and even orbitals. This mixing is relevant to the optical properties of transition metals in glasses and crystals and no method existed to determine this mixing before the advent of XNCD. Therefore, the calculation of optical spectra is usually made using incontrolable parameters to describe p-d mixing. Moreover, in optical spectroscopy, the signals coming from all elements in the sample are superimposed. In contrast, XNCD is element selective and the p-d mixing can be measured separately around each atomic species. The amount of p-d mixing is also important for the non-linear optical properties of crystals.

In X-ray absorption spectroscopy, the main thermal effect is represented by a Debye-Waller factor on the single-scattering contribution. Because of the absence of this contribution in XNCD spectra, and because of the slow convergence of the multiple-scattering series (Fig. 2) the action of disordered must be calculated on the full multiple-scattering expression. Therefore, XNCD provides a unique test of the multiple-scattering theories of disordered effects. In principle, the spectrum calculated at 0 K should be larger than the experimental spectrum at room temperature. This is not the case, maybe because inelastic effects are overestimated by our Hedin-Lundvist potential. Therefore, a study of XNCD spectra as a function of temperature is required to estimate the influence of thermal effects.

Finally, XNCD can be used to determine the chirality of a structure, as was demonstrated in the present example, where the comparison of experiment with calculation showed that the absolute configuration of our sample is the same as for the sample analyzed in reference [22].

We thank Prof. C. Malgrange for her help in the experiments and her very constructive comments. We are grateful to O.K. Andersen and O. Jepsen who made their LMTO program available to us. This work has been partially supported by EEC Contract ERBCHXCT90360.

References

1. J. Goulon, Ch. Goulon-Ginet, A. Rogalev, V. Gotte, C. Malgrange, Ch. Brouder, J. Chem. Phys. **108**, 6394 (1998).
2. L. Alagna, T. Prosperi, S. Turchini, J. Goulon, A. Rogalev, Ch. Goulon-Ginet, C.R. Natoli, R.D. Peacock, B. Stewart, Phys. Rev. Lett. **80**, 4799 (1998).
3. J. Goulon, *Rayonnement synchrotron polarisé, électrons polarisés et magnétisme*, edited by E. Beaurepaire, B. Carrière, J.-P. Kappler, (Strasbourg, IPCMS, 1989), p. 333.
4. L. Alagna, S. Di Fonzo, T. Prosperi, S. Turchini, P. Lazzaretti, M. Malagoli, R. Zazani, C.R. Natoli, P.J. Stephens, Chem. Phys. Lett. **223**, 402 (1994).
5. B. Stewart, J. Phys. IV France **4** C9-179 (1994).
6. Ch. Brouder, J. Phys.: Condens. Matter **2**, 597 (1990).
7. L. Mandel, Proc. Phys. Soc. Lond. **81**, 1104 (1963).
8. When the unit vector is complex, as is the case for circular polarization vectors, the spherical harmonics are calculated by replacing (x, y, z) by $(\epsilon_x, \epsilon_y, \epsilon_z)$ in the expression of the corresponding solid harmonics with $r = 1$ [9].
9. L.C. Biedenharn, J.D. Louck, *Angular Momentum in Quantum Physics* (Addison-Wesley, Reading, 1981).
10. D.A. Varshalovich, A.N. Moskalev, V.K. Khersonskii, *Quantum Theory of Angular Momentum* (World Scientific, Singapore, 1988).
11. M. Born, E. Wolf, *Principles of Optics* (Pergamon Press, Oxford, 1980).
12. B.T. Thole, P. Carra, F. Sette, G. van der Laan, Phys. Rev. Lett. **68**, 1943 (1992).
13. M. Altarelli, Phys. Rev. B **47**, 597 (1993).
14. P. Carra, B.T. Thole, M. Altarelli, X.-D. Wang, Phys. Rev. Lett. **70**, 694 (1993).

15. More precisely, the sum over f in equation (1) is over all the final states except the ground state. Therefore, $\sum_f |f\rangle\langle f| = 1 - |g\rangle\langle g|$. However, the matrix elements of the electric dipole and quadrupole operators between the ground state and the ground state are zero, because the core shell is full. The electronic relaxation around the core hole can modify this conclusion, but we neglect this effect here.
16. P. Strange, B.L. Gyorffy, Phys. Rev. B **52**, 13091 (1995).
17. M. Abramowitz, I.A. Stegun, *Handbook of Mathematical Functions* (Dover, New York, 1964).
18. Ch. Brouder, M.F. Ruiz López, R.F. Pettifer, M. Benfatto, C.R. Natoli, Phys. Rev. B **39**, 1488 (1989).
19. The other components of the tensor are $[\hat{\epsilon} \otimes \hat{\epsilon}^*]^{(2)}_{\pm 1} = \mp \Re(\epsilon_x \epsilon_z^*) - i\Re(\epsilon_y \epsilon_z^*)$ and $[\hat{\epsilon} \otimes \hat{\epsilon}^*]^{(2)}_{\pm 2} = \pm i\Re(\epsilon_x \epsilon_y^*) + (|\epsilon_x|^2 - |\epsilon_y|^2)/2$.
20. More generally, $\tau^{ij}(\ell\ell'; a\alpha) = (-1)^a \tau^{ji}(\ell'\ell; a\alpha)$, which is a consequence of the relation $\tau^{ij}_{\ell m \ell' m'} = (-1)^{m+m'} \tau^{ji}_{\ell' -m' \ell -m}$.
21. C.R. Natoli, M. Benfatto, S. Doniach, Phys. Rev. A **34**, 4682 (1986).
22. C. Svensson, J. Albertsson, R. Liminga, Å. Kvick, S.C. Abrahams, J. Chem. Phys. **78**, 7343 (1983).
23. L. Mattheiss, Phys. Rev. A **134**, 970 (1964).
24. E. Clementi, C. Roetti, Atom. Data Nucl. Data Tables **14**, 177 (1974).
25. P.A. Lee, G. Beni, Phys. Rev. B **15**, 2862 (1977).
26. L. Hedin, S. Lundqvist, *Effects of Electron-Electron and Electron-Phonon Interactions on the One-Electron States of Solids* (Academic Press, New York, 1969).
27. T.A. Tyson, K.O. Hodgson, C.R. Natoli, M. Benfatto, Phys. Rev. B **46**, 5997 (1992).
28. J.C. Fuggle, J.E. Inglesfield, *Unoccupied Electronic States* (Springer-Verlag, Berlin, 1992).
29. J.G. Jr Norman, Mol. Phys. **31**, 1191 (1976).
30. V. Briois, Ch. Brouder, Ph. Sainctavit, A. San Miguel, J.-P. Itié, A. Polian, Phys. Rev. B **56**, 5866 (1997).
31. V. Briois, Ch. Cartier, Ph. Sainctavit, Ch. Brouder, A.-M. Flank, J. Am. Chem. Soc. **117**, 1019 (1995).
32. I. Arčon, A. Kodre, M. Štuhec, D. Glavič-Gndro, W. Drube, Phys. Rev. A **51**, 147 (1995).